

# Large Scale Clustering of Sloan Digital Sky Survey Quasars: Impact of the Baryon Density and the Cosmological Constant

Kazuhiro YAHATA<sup>1</sup>, Yasushi SUTO<sup>1</sup>, Issha KAYO<sup>1,2</sup>, Takahiko MATSUBARA<sup>2</sup>,  
Andrew CONNOLLY<sup>3</sup>, Daniel VANDEN BERK<sup>3,4</sup>, Ravi SHETH<sup>3,5</sup>,  
István SZAPUDI<sup>6</sup>, Scott F. ANDERSON<sup>7</sup>, Neta BAHCALL<sup>8</sup>, Jon BRINKMANN<sup>9</sup>,  
István CSABAI<sup>10</sup>, Xiaohui FAN<sup>11</sup>, Jon LOVEDAY<sup>12</sup>,  
Alexander S. SZALAY<sup>10</sup>, and, Donald YORK<sup>13</sup>

<sup>1</sup>*Department of Physics, School of Science, The University of Tokyo, Tokyo 113-0033*

<sup>2</sup>*Department of Physics and Astrophysics, Nagoya University, Chikusa, Nagoya 161-8602*

<sup>3</sup>*University of Pittsburgh, Department of Physics and Astronomy,  
3941 O'Hara Street, Pittsburgh, PA 15260, USA*

<sup>4</sup>*Department of Astronomy and Astrophysics, Pennsylvania State University,  
525 Davey Laboratory, University Park, PA 16802, USA*

<sup>5</sup>*Department of Physics and Astronomy, University of Pennsylvania,  
Philadelphia, PA 15104, USA*

<sup>6</sup>*Institute for Astronomy, University of Hawaii,  
2680 Woodlawn Drive, Honolulu, HI 96822, USA*

<sup>7</sup>*Astronomy Department, University of Washington, Box 351580, Seattle, WA 98195, USA*

<sup>8</sup>*Princeton University Observatory, Peyton Hall, Princeton, NJ 08544, USA*

<sup>9</sup>*Apache Point Observatory, Sunspot, NM 88349-0059, USA*

<sup>10</sup>*Department of Physics and Astronomy, The Johns Hopkins University,  
3701 San Martin Drive, Baltimore, MD 21218, USA*

<sup>11</sup>*Steward Observatory, The University of Arizona, Tucson, AZ 85721, USA*

<sup>12</sup>*Astronomy Centre, University of Sussex, Falmer, Brighton BN1 9QJ, UK*

<sup>13</sup>*Astronomy and Astrophysics Department, University of Chicago,  
5640 South Ellis Avenue, Chicago, IL 60637, USA  
yahata@utap.phys.s.u-tokyo.ac.jp*

(Received 2004 December 3; accepted 2005 May 9)

## Abstract

We report the first result of the clustering analysis of Sloan Digital Sky Survey (SDSS) quasars. We compute the two-point correlation function (2PCF) of SDSS quasars in redshift space at  $8h^{-1}\text{Mpc} < s < 500h^{-1}\text{Mpc}$ , with particular attention to its baryonic signature. Our sample consists of 19986 quasars extracted from the SDSS Data Release 4 (DR4). The redshift range of the sample is  $0.72 \leq z \leq 2.24$  (the mean redshift is  $\bar{z} = 1.46$ ) and the reddening-corrected  $i$ -band apparent magnitude range is  $15.0 \leq m_{i,rc} \leq 19.1$ . Due to the relatively low number density of the quasar sample, the bump in the power spectrum due to the baryon density,  $\Omega_b$ , is not clearly visible. The effect of the baryon density is, however, to distort the overall shape of the 2PCF. The degree of distortion makes it an interesting alternate measure of the baryonic signature. Assuming a scale-independent linear bias and the spatially flat universe, i.e.,  $\Omega_b + \Omega_d + \Omega_\Lambda = 1$ , where  $\Omega_d$  and  $\Omega_\Lambda$  denote the density parameters of dark matter and the cosmological constant, we combine the observed quasar 2PCF and the predicted matter 2PCF to put constraints on  $\Omega_b$  and  $\Omega_\Lambda$ .

Our result is fitted as  $0.80 - 2.8\Omega_b < \Omega_\Lambda < 0.90 - 1.4\Omega_b$  at the  $2\sigma$  confidence level, which is consistent with results from other cosmological observations such as WMAP. The “mean” bias parameter of our quasar sample is  $1.59\sigma_8^{-1}$  (for  $\Omega_b = 0.04$  and  $\Omega_\Lambda = 0.7$ ), where  $\sigma_8$  is the top-hat mass fluctuation amplitude at  $8h^{-1}\text{Mpc}$ . We also estimate the corresponding bias parameter of quasars at  $z = 0$ ,  $b_{\text{QSO},\text{Fry}}(0)$ , assuming Fry’s bias evolution model. For  $\Omega_b = 0.04$ ,  $\Omega_\Lambda = 0.73$  and  $\Omega_d = 0.23$ , we find  $b_{\text{QSO},\text{Fry}}(0) = 0.54 + 0.83\sigma_8^{-1}$  which is valid for  $0.6 < \sigma_8 < 1.0$ .

**Key words:** galaxies: quasars: general — cosmology: large-scale structure of universe — cosmology: observations — methods: statistical

## 1. Introduction

Quasars are intrinsically bright and preferentially located at relatively high redshift. They are, therefore, naturally suited for exploring the structure of the distant universe out to redshifts  $z \sim 3$ , a regime not easily accessible from existing wide-field galaxy surveys. While surveys of the universe up to  $z \sim 6$  have significantly advanced in recent years using Lyman break-galaxies and Lyman- $\alpha$  emitters (e.g., Steidel et al. 1999; Shimasaku et al. 2003; Ouchi et al. 2004a; Ouchi et al. 2004b), they remain limited in terms of the areas they cover (barely extending to  $O(100)h^{-1}\text{Mpc}$ ). As such they are not well suited to measuring the large scale clustering at high redshift (i.e. they are sample variance limited). Quasar samples, in contrast, can be surveyed over very large volumes and, therefore, play an important and complementary role in measuring the evolution of structure in the universe on the largest accessible scales.

The primary goal of this quasar clustering analysis is to directly probe and quantify the large-scale structure of the universe on scales up to a few  $h^{-1}\text{Gpc}$ , where  $h$  denotes the Hubble constant in units of  $100\text{kms}^{-1}\text{Mpc}^{-1}$ . Eventually such analyses may enable us to answer fundamental questions including the homogeneity of the universe on Gpc scales or the validity of the cosmological principle (e.g., Lahav, Suto 2004). Also the clustering signal provides important clues to the formation and evolution of quasars themselves and may shed light on the growth history of their central massive black holes.

Although there are several seminal papers addressing quasar clustering (Osmer 1981; Shanks et al. 1987; Boyle, Mo 1993; Croom, Shanks 1996), those previous quasar samples were fairly small which limits their statistical power in constraining large scale structure. The 2dF QSO Redshift Survey (2QZ; Croom et al. 2001; Croom et al. 2002; Outram et al. 2003) and the SDSS are among the largest statistical samples which should significantly advance the statistics of quasar clustering analysis.

This is the first of a series of SDSS quasar clustering papers and is aimed at exploring the impact of the baryon density and the cosmological constant on the quasar 2PCF on scales of  $\sim 100h^{-1}\text{Mpc}$ . In this sense, our current approach is quite complementary to the existing galaxy clustering studies by the SDSS collaboration (e.g., Tegmark et al. 2004; Pope et al. 2004). The samples and techniques are complementary: the galaxies and quasars are selected using different algorithms, they explore vastly different volumes, the number densities of the objects are very different, and they cover very different redshift ranges. It would be interesting to see if both data sets yield consistent results on constraints on the cosmological parameters.

We will address the dependence of the quasar 2PCFs on redshift and luminosity and comparison with those of galaxies and AGNs in a separate paper (Connolly et al. 2005). To be specific, we compute the 2PCF of quasars from SDSS Data Release 4 (DR4) on scales from  $8h^{-1}\text{Mpc}$  to  $2h^{-1}\text{Gpc}$  and perform statistical analyses that pay particular attention to the embedded baryonic signature. From recent progress in the theoretical and observational understanding of the initial conditions present in the early universe, the 2PCF of the matter is well described. Two characteristic scales in the matter 2PCF,  $\xi_m(r, z)$ , are present at approximately  $100h^{-1}\text{Mpc}$ ; the baryon bump and the zero-crossing point (denoted by  $s_{\text{zero}}$  in what follows). These features are sensitive to the baryon density parameter,  $\Omega_b$ , and the matter density parameter,  $\Omega_m$ , where we define  $\Omega_m \equiv \Omega_b + \Omega_d$ , with  $\Omega_d$  being the density parameter of cold dark matter (CDM).

We derive constraints on  $\Omega_b$  and  $\Omega_\Lambda$  assuming a spatially flat universe (i.e.,  $\Omega_b + \Omega_d + \Omega_\Lambda = 1$ ) throughout this paper. Our attempt may be partially interpreted as yet another cosmological test to determine the values of  $\Omega_b$  and  $\Omega_\Lambda$  independent of existing methods. In this respect, our current results discussed below are not stringent enough to improve the previous constraints. Nevertheless we believe that the attempt to look for the baryonic signature in the cosmological distribution of quasars is of scientific interest on its own.

## 2. SDSS quasar sample

### 2.1. The Sloan Digital Sky Survey

The Sloan Digital Sky Survey (SDSS; York et al. 2000 for a technical summary) provides the largest homogeneous sample of quasars currently available, and thus is best suited for our current purpose. The wide-field five band photometric system (Gunn et al. 1998; Fukugita et al. 1996; Hogg et al. 2001; Ivezić et al. 2004; Smith et al. 2002) enables the identification of quasars with high efficiency and completeness. The precision astrometry (Pier et al. 2003) maintains the accuracy of the clustering analysis even in  $100h^{-1}\text{kpc}$  scale. The SDSS is also excellent in terms of the homogeneity of the spectroscopic sample because its spectroscopic targets are selected consistently on the basis of their photometric data. The details of quasar target selection algorithm are described by Richards et al. (2002), and the spectroscopic tiling algorithm is described by Blanton et al. (2003).

### 2.2. Quasar sample selection

The spectroscopic sample of quasars in the DR4 is selected according to several different spectroscopic target selection criteria (see Table 27 of Stoughton et al. 2002). We consider only the point sources, and extract our quasar sample

for the current analysis on the basis of four conditions; first, to ensure a homogeneity of the sample, we choose those spectroscopic quasars whose “primTarget” flag (see Table 6 of Stoughton et al. 2002) indicates either “QSO\_CAP” or “QSO\_SKIRT” (see Fig.1 and section 3.4 of Richards et al. 2002). Second, their  $i$ -band magnitude corrected for the Galactic reddening should satisfy  $15.0 < m_{i,rc} < 19.1$ , which are the limits used by the quasar target selection algorithm. We adopt the reddening correction of Schlegel, Finkbeiner, Davis (1998). Although this correction is calculated adopting the typical spectrum energy distribution of elliptical galaxies and the old SDSS filter response functions the resulting difference is negligibly small. Third, the redshift limits of this sample are  $0.72 < z < 2.24$ . In the SDSS photometric system, the color locus of quasars in the redshift range  $2.4 < z < 3.0$  crosses the stellar locus and thus the survey completeness becomes significantly degraded in that redshift range. This defines the upper redshift limit of our sample. The lower limit is chosen so that the absolute magnitude of all the selected quasars should be brighter than  $-23$  in  $i$ -band. Finally, we exclude the southern sky region because the selection of the region is different from that of the northern sky. The total number of selected quasars is 19986.

The SDSS photometric data have two different versions; “BEST” version denotes the highest quality data at the time of the data release, while “TARGET” version is the data at the time the target selection algorithm was run for that part of the sky (i.e., the photometric data may be updated at the time of the data release). Our current sample uses the “primTarget” flag which is based on the “TARGET” version. In reality, however, the two versions may lead to some systematic effect due to the mismatch of the time-dependent selection function. We compared BEST and TARGET using the SDSS Data Release 3 (DR3: see Abazajian et al. 2004) QSO catalog (Schneider et al. 2005), and found that the difference does not affect the resulting 2PCFs within the current errorbars (see Fig.4 below). We note that our sample in the DR3 region slightly differs from DR3 QSO catalog (Schneider et al. 2005) because we have not manually inspected all objects classified by the *pipeline* as quasars. The number of quasars in a subset of our DR4 sample that is located in the DR3 region is 16656, out of which 32 objects are not listed in the catalog of Schneider et al. (2005) and 9 objects have incorrect redshifts. This difference of the quasar samples, however, has a negligible effect on the estimated 2PCF as will be shown below.

The equatorial coordinate distribution of our quasar sample is plotted in Figure 1, and a projected wedge diagram of the quasars is shown in Figure 2. Figure 3 shows the scatter plot of redshift and  $i$ -band absolute magnitude (*Upper panel*) and the redshift histogram (*Lower panel*).

Giving the errorbars in Fig.4, the photometric completeness, fiber collisions and the effect of errors in the reddening correction are not supposed to change our result. Those issues will be fully addressed by Connolly et al. (2005) who found that none appears to significantly affect the quasar 2PCFs presented below.

### 2.3. Analysis

We use the Landy-Szalay estimator (Landy, Szalay 1993) in computing the 2PCF from the quasar sample:

$$\xi_{\text{QSO,obs}}(s_i \leq s < s_{i+1}) = \frac{QQ(s_i \leq s < s_{i+1})}{RR(s_i \leq s < s_{i+1})} - 2 \frac{QR(s_i \leq s < s_{i+1})}{RR(s_i \leq s < s_{i+1})} + 1, \quad (1)$$

where  $QQ$ ,  $QR$ , and  $RR$  are the number of corresponding pairs of quasars and random particles that are normalized by  $N_Q(N_Q - 1)/2$ ,  $N_Q N_R$ ,  $N_R(N_R - 1)/2$ , respectively ( $N_Q$  and  $N_R$  are the numbers of quasars and random particles). The accuracy and convergent properties of the Landy – Szalay estimator are discussed in the appendix of Kayo et al. (2004) and in Kerscher, Szapudi & Szalay (2000).

The redshift distribution of random particles is determined so as to reproduce that of the quasars. The latter is estimated by averaging over a finite width of redshift,  $\Delta z = 0.08$ . We find that other choices of  $\Delta z = 0.02$ ,  $\Delta z = 0.04$  and  $\Delta z = 0.10$  result in almost identical  $\xi_{\text{QSO,obs}}(s)$ . The number of random particles,  $N_R$ , is about 600,000, which is found to provide robust estimates of  $\xi_{\text{QSO,obs}}(s)$  on the scales  $s > 8h^{-1}\text{Mpc}$ . We evaluate the covariance matrix,  $C_{ij}$ , from 40 jack-knife re-samplings (see e.g., Lupton 1993). In order to ensure the statistical significance, the comparison between the observed and the predicted 2PCFs needs to be done after the finite binning of the pair-separation. Empirically, we compute the 2PCFs at 6 different binning offsets; the  $i$ -th boundary of the  $n$ -th binning offset ( $n = 1 \dots 6$ ) is defined as

$$s_i(n) = 10^{0.3i+0.05(n-1)} h^{-1} \text{Mpc}. \quad (2)$$

We then compute the averaged 2PCFs of theoretical predictions (described in section 3) as follows:

$$\xi_{\text{QSO}}(s_i \leq s < s_{i+1}) = \frac{\int_{s_i}^{s_{i+1}} \xi_{\text{QSO}}(s') s'^2 ds'}{\int_{s_i}^{s_{i+1}} s'^2 ds'}. \quad (3)$$

In practice, for a given  $n$ -th offset of the binning, we use bins whose boundaries satisfy  $7.9h^{-1}\text{Mpc} < s_i < 502h^{-1}\text{Mpc}$  for the following analysis. Figure 4 plots the 2PCFs of our samples for the  $n = 1$  binning offset adopting  $\Omega_m = 0.3$ ,  $\Omega_\Lambda = 0.7$  and  $h = 0.7$ . We also plot the 2PCFs of a subset of our DR4 sample that is located in the DR3 region, and two 2PCFs of BEST and TARGET samples of the DR3 quasar catalog (Schneider et al. 2005) for comparison. The four sets of 2PCFs agree with one another to within  $1\sigma$ . Throughout the paper, we show the 2PCFs in log-log plots.

In order to show the negative part of 2PCFs, we plot the range of  $-10^{-2} < \xi < -10^{-5}$  in the lower panel of each figure by taking the logarithm of its absolute value.

### 3. Theoretical predictions

#### 3.1. Parameter dependence of the matter 2PCF

Since the baryon bump is the counterpart of the acoustic oscillation peaks in a matter power spectrum, the analysis using the 2PCF should, in principle, be equivalent to that with the power spectrum. Nevertheless we perform the analysis with the 2PCF for the following two reasons. The first advantage is based on the different behavior of the baryonic signature in the power spectrum and 2PCF. While the acoustic oscillation peaks in a matter power spectrum show up in several overtones, they translate coherently to the baryon bump in the 2PCF roughly at one specific scale. Thus the resulting signature is expected to be more prominent in the 2PCF. The second is related to the inevitably complicated geometry of the survey volume boundary. Strictly speaking, the estimate of the power spectrum from the observed sample has to assume a periodic boundary condition unless resorting to a very sophisticated estimation methodology (e.g., Pope et al. 2004). On the other hand, the 2PCF can be reliably estimated by taking account of the arbitrary boundary shape of the survey volume in a relatively straightforward fashion. For this purpose, we simply distribute random particles over the survey volume according to the selection function of quasars (the lower-panel of Fig.3) and perform standard pair-counting. This is why we adopt the 2PCF in the present analysis.

In locating the baryon bump and the zero-crossing point, it is important to have accurate predictions of the matter 2PCF. Here we adopt an empirical fitting formula for the CDM transfer function incorporating the effect of  $\Omega_b$  (Eisenstein, Hu 1998). The theoretical model of 2PCFs depends on  $\Omega_m$  and  $\Omega_b$  and not on  $\Omega_\Lambda$ , while the estimate of the observed 2PCFs requires the values of  $\Omega_m$  and  $\Omega_\Lambda$ . To simplify the analysis, therefore, we adopt a spatially-flat universe,  $\Omega_m + \Omega_\Lambda = 1$ , and choose  $\Omega_b$  and  $\Omega_\Lambda$  as two model parameters.

Figure 5 shows  $\xi_m(r, z=0)$  for different values of  $\Omega_b$  ( $\Omega_\Lambda$  is fixed to 0.73). Baryon bumps are always visible around  $100h^{-1}\text{Mpc}$  (except for the case of  $\Omega_b = 0$ ) and their height and position are sensitive to the value of  $\Omega_b$ . Figure 6 also plots  $\xi_m(r, z=0)$  but for different values of  $\Omega_\Lambda$  assuming  $\Omega_b = 0.04$ . It is clear that  $s_{\text{zero}}$  is very sensitive to  $\Omega_\Lambda$  and, to a lesser extent, to  $\Omega_b$ .

Figure 7 shows the dependence of  $\xi_m(r, z=0)$  on  $h$ . Interestingly,  $s_{\text{zero}}$  is quite insensitive to the value of the Hubble constant. If  $\Omega_b = 0$ , the CDM linear matter spectrum is approximately given as a universal function of the scaled wavenumber,  $q \equiv k/(\Omega_m h^2)$  implying the scaling of  $s_{\text{zero}}[h^{-1}\text{Mpc}] \propto (\Omega_m h)^{-1}$  (see also Matsubara 2004 for related discussion on the parameter dependence). We made sure that this scaling holds for  $\Omega_b < 0.01$  but is replaced by a different empirical relation of  $s_{\text{zero}}[h^{-1}\text{Mpc}] \propto \Omega_m^{-1} = (1 - \Omega_\Lambda)^{-1}$  for  $\Omega_b > 0.02$  (the second equality comes from our assumption of the spatially flat universe). We note here that the above feature may be very useful in breaking the degeneracy in the constraints on  $\Omega_m$  and  $h$ .

#### 3.2. Predicting 2PCF of quasars on the light-cone

In order to predict the observable 2PCF of quasars  $\xi_{\text{QSO}}(s)$  from the matter 2PCF  $\xi_m(r, z)$ , one has to take into account three major effects, (i) the light-cone effect, (ii) redshift-space distortion and (iii) quasar biasing. Since the formulation and the prescription of incorporating these effects have been extensively discussed in the literature (Yamamoto, Suto 1999; Suto et al. 1999; Hamana, et al. 2001; Hamana et al. 2001; Lahav, Suto 2004), we simply summarize the results below.

##### 3.2.1. Light-cone effect

Since the current quasar sample extends from  $z = 0.72$  to  $z = 2.24$ , the clustering evolution within the survey volume cannot be neglected; for instance, the linear growth rate of density fluctuations,  $D(z)$ , in the universe with  $\Omega_m = 0.27$  and  $\Omega_\Lambda = 0.73$  varies from  $D(0)/D(0.72) = 1.41$  to  $D(0)/D(2.24) = 2.49$ . This implies that the corresponding matter 2PCF in the linear regime evolves by a factor of  $[D(0.72)/D(2.24)]^2 \approx 3.1$  between the two edges of the survey volume. Although we could reduce the effect in principle by dividing the entire sample into several subsamples in a narrow redshift range, it would appreciably degrade the statistical significance of the result. This is why one has to carry out the proper averaging procedure in predicting  $\xi_{\text{QSO}}(s)$  theoretically. To be specific, we follow the formula described by Hamana, et al. (2001):

$$\xi_{\text{QSO}}(s) = \frac{\int_{z_{\text{min}}}^{z_{\text{max}}} dz \frac{dV_c}{dz} [\phi(z)n_0(z)]^2 \xi_{\text{QSO}}(s, z)}{\int_{z_{\text{min}}}^{z_{\text{max}}} dz \frac{dV_c}{dz} [\phi(z)n_0(z)]^2}, \quad (4)$$

where  $z_{\text{min}}$  and  $z_{\text{max}}$  denote the redshift range of the survey,  $dV_c/dz$  is the differential comoving volume element,  $\phi(z)$  is the selection function of quasars,  $n_0(z)$  is the number density of quasars, and  $\xi_{\text{QSO}}(s, z)$  is the 2PCF of quasars in

redshift space at  $z$ .

In practice, we rewrite equation (4) as

$$\xi_{\text{QSO}}(s) = \frac{\int_{z_{\text{min}}}^{z_{\text{max}}} dz \left(\frac{dV_c}{dz}\right)^{-1} \left(\frac{dN_{\text{QSO}}(z)}{dz}\right)^2 \xi_{\text{QSO}}(s, z)}{\int_{z_{\text{min}}}^{z_{\text{max}}} dz \left(\frac{dV_c}{dz}\right)^{-1} \left(\frac{dN_{\text{QSO}}(z)}{dz}\right)^2}. \quad (5)$$

In the above expression,  $dN_{\text{QSO}}(z)/dz$  is the redshift number distribution of quasars which is directly estimated from the data (Lower panel of Fig.3), and  $dV_c/dz$  can be easily computed once a set of cosmological parameters is specified.

### 3.2.2. Redshift-space distortion

The next task is to convert the theoretical predictions in real space to those in redshift space. Since the current paper focuses on scales beyond  $\sim 10h^{-1}\text{Mpc}$ , the nonlinear effect (i.e., fingers of god) is not important and we may just consider the Kaiser effect (Kaiser 1987):

$$\xi_{\text{QSO}}(s, z) = \left(1 + \frac{2}{3}\beta(z) + \frac{1}{5}\beta^2(z)\right) \xi_{\text{QSO}}(r, z), \quad \beta(z) \equiv \frac{1}{b_{\text{QSO}}(z)} \frac{d \ln D(z)}{d \ln a}, \quad (6)$$

where  $r$  and  $s$  denote the quasar pair-separations (comoving) in real and redshift spaces, respectively,  $a$  is the scale factor, and  $b_{\text{QSO}}(z)$  is the biasing factor of quasars at  $z$  as described below. This expression assumes the distant-observer approximation, and can be justified for pair-separations less than  $10^\circ$  on the sky (Matsubara 2000). For reference, at the median redshift of  $z \sim 1.4$ , the comoving scale subtended by an angle of  $10^\circ$  is  $\approx 511h^{-1}\text{Mpc}$  in the  $\Omega_m = 0.3$  and  $\Omega_\Lambda = 0.7$  model. This is why we only use the bins less than  $502 h^{-1}\text{Mpc}$  where the distant-observer approximation can be reasonably justified.

### 3.2.3. Quasar biasing

The quasar biasing could be fairly complex in principle, but again in the linear regime that we consider here, one can safely assume the scale-independent and linear bias (e.g., Matsubara 1999):

$$\xi_{\text{QSO}}(r, z) = [b_{\text{QSO}}(z)]^2 \xi_m(r, z) = [b_{\text{QSO}}(z)]^2 D(z)^2 \xi_m(r, 0). \quad (7)$$

Then it should be emphasized here that all the above three effects (the light cone effect, the redshift-space distortion, and the quasar biasing) are linear in a sense that equations (5) to (7) yield a linear relation between the quasar 2PCF in redshift space on the light-cone and the matter 2PCF in real space at  $z = 0$ . In particular the three effects simply change the amplitude of the matter 2PCF but none changes the positions of the baryon bump and the zero-crossing scale. This is valid only in the linear regime, and significantly simplifies the analysis. Consequently we can simply introduce an effective biasing factor,  $b_{\text{eff}}$ :

$$\xi_{\text{QSO}}(s) = b_{\text{eff}}^2 \xi_m(r, 0), \quad (8)$$

and

$$b_{\text{eff}}^2 = \frac{\int_{z_{\text{min}}}^{z_{\text{max}}} dz \left(\frac{dV_c}{dz}\right)^{-1} \left(\frac{dN_{\text{QSO}}(z)}{dz}\right)^2 \left(1 + \frac{2}{3}\beta(z) + \frac{1}{5}\beta^2(z)\right) b_{\text{QSO}}^2(z) D^2(z)}{\int_{z_{\text{min}}}^{z_{\text{max}}} dz \left(\frac{dV_c}{dz}\right)^{-1} \left(\frac{dN_{\text{QSO}}(z)}{dz}\right)^2}. \quad (9)$$

We note a possible systematic effect that gives rise to scale-dependence in the effective bias: if mean redshifts of quasar pairs which contribute to small-scale and large-scale correlations are significantly different, the biasing measured on the light-cone may acquire artificial scale-dependence. In other words, the redshift dependence of the selection function combined with that of the *scale-independent* bias may induce additional scale-dependence in the effective bias. For instance, Tegmark et al. (2004) discussed in detail how the luminosity dependence yields such scale-dependence of biasing using a subset of the DR2 SDSS galaxy catalog. In the current sample, however, this is not a serious problem for two reasons. First, while the luminosity and color dependence of galaxy clustering is well established (Kayo et al. 2004; Zehavi et al. 2004), it is not yet clear that quasars also exhibit similar strong dependence on their intrinsic properties. Croom et al. (2004), for instance, find no significant luminosity dependence in the clustering of 2dF QSOs. Second, as is clear from the QSO distribution plot and  $dN/dz$  (Figs. 1 and 2), all separation bins of the 2PCF that we use in the analysis are not dominated by those in any specific redshift range, rather they are contributed equally over the entire redshift range. To be more specific, we compute the mean redshifts of pairs,  $\bar{z}$ , at separation bins of  $s$  assuming  $\Omega_m = 0.3$  and  $\Omega_\Lambda = 0.7$ . We find  $(\bar{z}, s) = (1.40, 13h^{-1}\text{Mpc}), (1.41, 25h^{-1}\text{Mpc}), (1.41, 100h^{-1}\text{Mpc}), (1.41,$

$200h^{-1}\text{Mpc}$ ),  $(1.41, 400h^{-1}\text{Mpc})$ ,  $(1.42, 800h^{-1}\text{Mpc})$ , and  $(1.41, 1600h^{-1}\text{Mpc})$ . This reasonably justifies the fact that we neglect the luminosity dependence of quasar biasing.

Thus we proceed as follows; first we specify the values of  $\Omega_b$ ,  $\Omega_\Lambda$ , and  $h$ , then compute  $\xi_m(r, 0)$ . Since we assume the spatially flat model,  $\Omega_m$  is given as  $1 - \Omega_\Lambda$ . As discussed below, we do not have to specify the value of  $\sigma_8$ , the top-hat mass fluctuation amplitude at  $8h^{-1}\text{Mpc}$ , as long as we do not intend to solve for  $b_{\text{QSO}}(z)$ . Second we evaluate  $\xi_{\text{QSO}}(s)$  from the quasar sample using the same values of  $\Omega_m$ ,  $\Omega_\Lambda$ , and  $h$ . Finally, we compute the  $\chi^2$  of the observed and the model 2PCFs by varying the value of  $b_{\text{eff}}$ . In doing so, we use both diagonal and off-diagonal elements of the covariance matrix:

$$\chi^2 = \sum_{ij} (\xi_{\text{QSO,obs},i} - b_{\text{eff}}^2 \xi_{m,i}) (\xi_{\text{QSO,obs},j} - b_{\text{eff}}^2 \xi_{m,j}) C_{ij}^{-1}, \quad (10)$$

where  $C_{ij}^{-1}$  is the inverse matrix of the covariance matrix and the subscripts,  $i$  and  $j$ , are indices of separation bins. We repeat the above procedure for  $0 < \Omega_b < 1$  and  $0 < \Omega_\Lambda < 1$ , and derive constraints on the two parameters. We adopt  $h = 0.7$  as a fiducial value, but also show results for  $h = 0.6$  and  $h = 0.8$  as well, although the  $h$ -dependence is very weak.

The resulting constraints are independent of the value of  $\sigma_8$  and also of the evolution model of  $b_{\text{QSO}}(z)$ . Nevertheless it is also interesting to estimate the quasar biasing factor even in a model-dependent manner. We adopt a simple evolution model by Fry (1996):

$$b_{\text{QSO}}(z) = 1 + \frac{b_{\text{QSO}}(z=0) - 1}{D(z)}, \quad (11)$$

This model neglects the possible luminosity/color dependence of quasar biasing and the finite lifetime of quasars, and may need to be improved to some extent; we note that Croom et al. (2004) find no significant luminosity dependence in the clustering of 2dF QSOs. Nevertheless equation (11) gives us a useful measure of the expected degree of the quasar spatial biasing at  $z = 0$ .

#### 4. Results and Discussion

In performing the statistical analysis, we recompute  $\xi_{\text{QSO,obs}}(s)$  for different values of  $\Omega_\Lambda$  ( $0 < \Omega_\Lambda < 1$  at an interval of  $\Delta\Omega_\Lambda = 0.05$ ). Figure 8 shows the observed 2PCFs of the SDSS quasars for several different values of  $\Omega_\Lambda$  (the  $n = 1$  binning offset). Each data point and associated errorbar is slightly shifted horizontally for clarity. Unlike in Figures 5 to 7, the baryon bump is not directly visible due to the large bin size. Because of the statistical limitation, we also do not directly detect the anti-correlation that is predicted beyond a scale of  $200h^{-1}\text{Mpc}$  (in the case of  $\Omega_b = 0.04$  and  $\Omega_\Lambda = 0.7$  universe). However, we find that there is a break in the slope of the 2PCF around  $100h^{-1}\text{Mpc}$ . While  $\xi_{\text{QSO,obs}}(s)$  is always positive on the scales less than  $100 h^{-1}\text{Mpc}$ , it is not inconsistent to be negative on the larger scale for any sets of cosmological parameters that we surveyed here. Thus this break may be interpreted to put a lower limit on the zero-crossing scale of  $\xi_{\text{QSO,obs}}(s)$ .

Figure 9 shows the 2PCFs of SDSS quasars using the 6 different binning offsets ( $\Omega_m = 0.3$  and  $\Omega_\Lambda = 0.7$ ). The break of  $\xi_{\text{QSO,obs}}(s)$  around  $100h^{-1}\text{Mpc}$  is quite robust against the different choice of the binning. Since the data at different bins are strongly correlated, we do not use this entire dataset for our analysis; this is just to show that the binning makes little difference. In what follows, we perform statistical analysis for the  $n = 1$  and  $n = 4$  offsets, separately.

Figure 10 shows the corresponding contours of

$$\Delta\chi^2(\Omega_b, \Omega_\Lambda) \equiv \chi^2(\Omega_b, \Omega_\Lambda, b_{\text{eff,min}}) - \chi_{\text{min}}^2, \quad (12)$$

where  $b_{\text{eff,min}}$  is the value of  $b_{\text{eff}}$  which minimizes  $\chi^2$  for a given set of  $\Omega_b$  and  $\Omega_\Lambda$ , and  $\chi_{\text{min}}^2$  is the global minimum value in  $\Omega_b$ ,  $\Omega_\Lambda$  and  $b_{\text{eff}}$  parameter space. The three curves represent the 68%, 95% and 99.7% confidence levels. Figure 11 is the same plot but employs the  $n = 4$  binning offset (see Fig. 9).

The cosmological parameters inferred from the WMAP results (Spergel et al. 2003) are in agreement with our constraints in Figures 10 and 11 at the 68% confidence level. Given these uncertainties, therefore, we express our constraints as allowed regions of  $\Omega_b$  and  $\Omega_\Lambda$ . For this purpose, we fit the mean and  $2\sigma$  contours as straight lines and obtain

$$2.1\Omega_b + \Omega_\Lambda = 0.89 \quad (\text{mean}), \quad (13)$$

$$0.80 - 2.8\Omega_b < \Omega_\Lambda < 0.90 - 1.4\Omega_b \quad (2\sigma) \quad (14)$$

for the  $n = 1$  binning offset (Fig. 10), and

$$3.6\Omega_b + \Omega_\Lambda = 0.99 \quad (\text{mean}), \quad (15)$$

$$0.69 - 5.1\Omega_b < \Omega_\Lambda < 1.0 - 2.3\Omega_b \quad (2\sigma) \quad (16)$$

for the  $n = 4$  binning offset (Fig. 11). These fitted lines are also plotted in Figures 10 and 11. The differences of the slopes of contours between the  $n = 1$  and  $n = 4$  binning offsets mainly come from the smallest-scale behavior of  $\xi_{\text{QSO,obs}}(s)$ , but the resulting constraints are fairly insensitive to the different binning offsets (compare Figs. 10 and 11). The dependence of our constraints on the Hubble constant is illustrated in Figure 12. The upper and lower panels are derived by employing the  $n = 1$  and  $n = 4$  offsets, respectively. The left and right panels show the results for  $h = 0.6$ , and  $h = 0.8$ , and the central panels plot the results for  $h = 0.7$  (identical to Figures 10 and 11) for comparison. Except for the small difference, the overall conclusion is that our constraints are very insensitive to the choice of  $h$ .

Finally, let us consider the corresponding biasing parameter of quasars implied from the current study. Unfortunately the current sample cannot constrain the redshift-dependence on the bias evolution. Thus we have to specify the value of  $\sigma_8$  (at  $z=0$ ) and the evolution model of quasar biasing as well, although all the constraints presented above are independent of those assumptions. For simplicity and clarity, we adopt  $\Omega_b = 0.04$  and  $\Omega_\Lambda = 0.70$ . Then we find that  $b_{\text{eff}}$  is  $1.13\sigma_8^{-1}$  for  $0.6 < \sigma < 1.0$ . If we define a ‘‘mean’’ quasar bias as

$$b_{\text{mean}}^2 = b_{\text{eff}}^2 \left[ \frac{\int_{z_{\text{min}}}^{z_{\text{max}}} dz \left( \frac{dV_c}{dz} \right)^{-1} \left( \frac{dN_{\text{QSO}}(z)}{dz} \right)^2 \left( 1 + \frac{2}{3}\beta(z) + \frac{1}{5}\beta^2(z) \right) D^2(z)}{\int_{z_{\text{min}}}^{z_{\text{max}}} dz \left( \frac{dV_c}{dz} \right)^{-1} \left( \frac{dN_{\text{QSO}}(z)}{dz} \right)^2} \right]^{-1}, \quad (17)$$

we find that  $b_{\text{mean}} = 1.59\sigma_8^{-1}$  (the mean redshift of the sample is  $z_{\text{is}} = 1.46$ ). This is a measure of the degree of quasar clustering if the quasar biasing is *independent of redshift*. We think this result is consistent with Croom et al. 2004. If we adopt another bias evolution (eq.[11]) instead, the current quasar sample is fitted to have  $b_{\text{QSO,Fry}}(z = 0) = 0.54 + 0.83\sigma_8^{-1}$ .

## 5. Summary

We have presented the first result of the SDSS quasar clustering analysis. In particular we have focused on the behavior of the quasar two-point correlation functions (2PCF) at large scales, and explored the embedded baryonic signature through the overall shape of the quasar 2PCF. The measurement is still statistically limited, but we found that the zero-crossing scale of the quasar 2PCFs is larger than  $100h^{-1}\text{Mpc}$ . The estimated quasar 2PCFs are in good agreement with those predicted in linear theory combining the light-cone effect, the redshift-space distortion and the scale-independent linear biasing model.

To proceed further, we have attempted to derive joint constraints on the baryon density parameter  $\Omega_b$  and the cosmological constant  $\Omega_\Lambda$  under the assumption of the spatially flat universe. Our constraints are approximately expressed by the relation:  $0.80 - 2.8\Omega_b < \Omega_\Lambda < 0.90 - 1.4\Omega_b$  at the  $2\sigma$  confidence level ( $n = 1$  binning offset). While the statistical significance is not competitive, the constraint is consistent with the independent results from other observations such as WMAP (Spergel et al. 2003) within the  $1\sigma$  level.

The current analysis can be improved in many different ways; to consider non-flat ( $\Omega_m + \Omega_\Lambda \neq 1$ ) models, to explore a more general equation of state of the universe than the cosmological constant (e.g., Yamamoto 2004), to consider the anisotropy of the 2-dimensional correlation function (Matsubara, Suto 1996), to incorporate the gravitational nonlinearity effect which is not important on  $\sim 10h^{-1}\text{Mpc}$  scales but still cannot be entirely neglected (Changbom Park, private communication), to take into account the finite angular size of the pair-separation (i.e., without adopting the distant-observer approximation; see Matsubara 2000), and to elaborate on the statistical modeling, in particular, the error estimation. We plan to perform such improved analyses in due course.

The wedge diagram of the current quasar sample, Figure 2, clearly illustrates the isotropy and homogeneity of the universe viewed over large scales, in marked contrast to the complex clustering pattern of the local universe traced by galaxies (e.g., Fig. 3 in Hikage et al. 2003). Therefore the most impressive lesson that we have learned from the current analysis may be the fact that we can indeed decipher cosmological information on  $\Omega_b$  and  $\Omega_\Lambda$  which is imprinted in the apparently almost homogeneous distribution of quasars at such high redshifts.

We thank Masamune Oguri, Changbom Park and Edwin L. Turner for useful discussions. This research was supported in part by Grants-in-Aid for Scientific Research from the Japan Society for Promotion of Science (Nos.14102004 and 16340053). AJC is partially supported by an NSF CAREER grant AST9984924 and an NSF ITR grant 1120201.

Funding for the creation and distribution of the SDSS Archive has been provided by the Alfred P. Sloan Foundation, the Participating Institutions, the National Aeronautics and Space Administration, the National Science Foundation, the U.S. Department of Energy, the Japanese Monbukagakusho, and the Max Planck Society. The SDSS Web site is <http://www.sdss.org/>.

The SDSS is managed by the Astrophysical Research Consortium (ARC) for the Participating Institutions. The Participating Institutions are The University of Chicago, Fermilab, the Institute for Advanced Study, the Japan Participation Group, The Johns Hopkins University, the Korean Scientist Group, Los Alamos National Laboratory, the

Max-Planck-Institute for Astronomy (MPIA), the Max-Planck-Institute for Astrophysics (MPA), New Mexico State University, University of Pittsburgh, Princeton University, the United States Naval Observatory, and the University of Washington.

## References

- Abazajian, K., et al. 2004, AJ, submitted (astro-ph/0410239)
- Blanton, M. R., Lupton, R.H., Maley, F.M., Young, N., Zehavi, I., & Loveday, J. 2003, AJ, 125, 2276
- Boyle, B. J. & Mo, H. J. 1993, MNRAS, 260, 925
- Connolly, A. et al. 2005, in preparation
- Croom, S. M., Shanks, T. 1996, MNRAS, 281, 893
- Croom, S. M., Shanks, T., Boyle, B. J., Smith, R. J., Miller, L., Loaring, N. S. & Hoyle, F. 2001, MNRAS, 325, 483
- Croom, S. M., Boyle, B. J., Loaring, N. S., Miller, L., Outram, P. J., Shanks, T., & Smith, R. J. 2002, MNRAS, 335, 459
- Croom, S. M., et al. 2005, MNRAS, 356, 415
- Eisenstein, D. J., & Hu, W. 1998, ApJ, 496, 605
- Fukugita, M., Ichikawa, T., Gunn, J.E., Doi, M., Shimasaku, K., & Schneider, D.P. 1996, AJ, 111, 1748
- Fry, N. J., 1996, ApJ, 461, L65
- Gunn, J. E., et al. 1998, AJ, 116, 3040
- Hamana, T., Colombi, S., & Suto, Y. 2001, A&A367, 18
- Hamana, T., Yoshida, N., Suto, Y., & Evrard, A. E. 2001 ApJL, 561, 143
- Hikage, C., et al. 2003, PASJ, 55, 911
- Hogg, D. W., Schlegel, D. J., Finkbeiner, D. P., & Gunn, J. E. 2001, AJ, 122, 2129
- Ivezic, Z., et al. 2004, AN, 325, 583
- Kaiser, N. 1987, MNRAS, 227, 1
- Kayo, I., et al. 2004, PASJ, 56, 415
- Kerscher, M., Szapudi, I., & Szalay, A. S. 2000, ApJ, 535, L13
- Landy, S. D. & Szalay, S. 1993, ApJ, 412, 64
- Lahav, O. & Suto, Y. 2004, Liv. Rev. Rela. 7, 8
- Lupton, R. H. 1993, Statistics in Theory and Practice (Princeton: Princeton Univ. Press)
- Matsubara, T. 1999, ApJ, 525, 543
- Matsubara, T. 2000, ApJ, 535, 1
- Matsubara, T. 2004, ApJ, in press (astro-ph/0408349)
- Matsubara, T. & Suto, Y. 1996, ApJ, 470, L1
- Osmer, P. S. 1981, ApJ, 247, 762
- Ouchi, M. et al. 2004a, ApJ, 611, 660
- Ouchi, M. et al. 2004b, ApJ, 611, 685
- Outram, P. J., Hoyle, F., Shanks, T., Croom, S. M., Boyle, B. J., Miller, L., Smith, R. J. & Myers, A. D. 2003, MNRAS, 342, 483
- Pier, J. R., Munn, J. A., Hindsley, R. B., Hennessy, G. S., Kent, S. M., Lupton, R. H., & Ivezić, Z. 2003, AJ, 125, 1559
- Pope, A. C., et al. 2004, ApJ, 607, 655
- Richards, G. T., et al. 2002, AJ, 123, 2945
- Schlegel D. J., Finkbeiner, D., & Davis, M. 1998, ApJ, 500, 525
- Schneider, D. P., et al. 2005, AJ, in press (astro-ph/0503679)
- Shanks, T., Fong, R., Boyle, B. J., & Peterson, B. A. 1987, MNRAS, 227, 739
- Shimasaku, K. et al. 2003, ApJ, 586, L111
- Smith, J., et al. 2002, AJ, 123, 2121
- Spergel, D. N. et al. 2003, ApJS, 148, 175
- Steidel, C. C., Adelberger, K. L., Giavalisco, M., Dickinson, M., & Pettini, M., 1999, ApJ, 519, 1
- Stoughton, C., et al. 2002, AJ, 123, 485
- Suto, Y., Magira, H., Jing, Y. P., Matsubara, T., & Yamamoto, K., 1999, Prog. Theor. Phys. Suppl., 133, 183
- Tegmark, M., et al. 2004, ApJ, 606, 702
- Yamamoto, K. 2004, ApJ, 605, 620
- Yamamoto, K., & Suto, Y., 1999, ApJ, 517, 1
- York, D. G., et al. 2000, AJ, 120, 1579
- Zehavi, I. et al. 2004, submitted to ApJ(astro-ph/0408569)



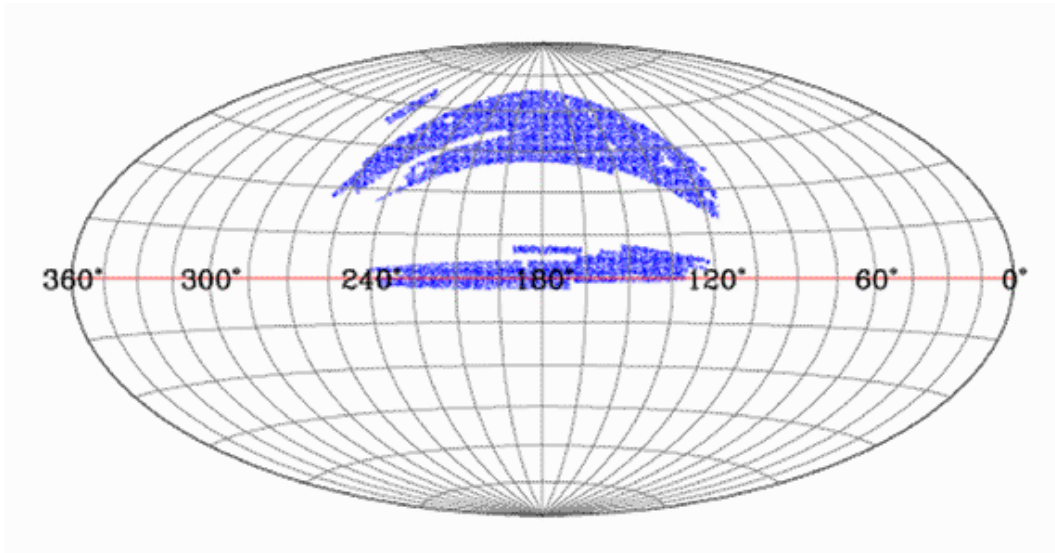


Fig. 1. Equatorial coordinate distribution of SDSS quasars that we use in the current analysis (19986 in total).

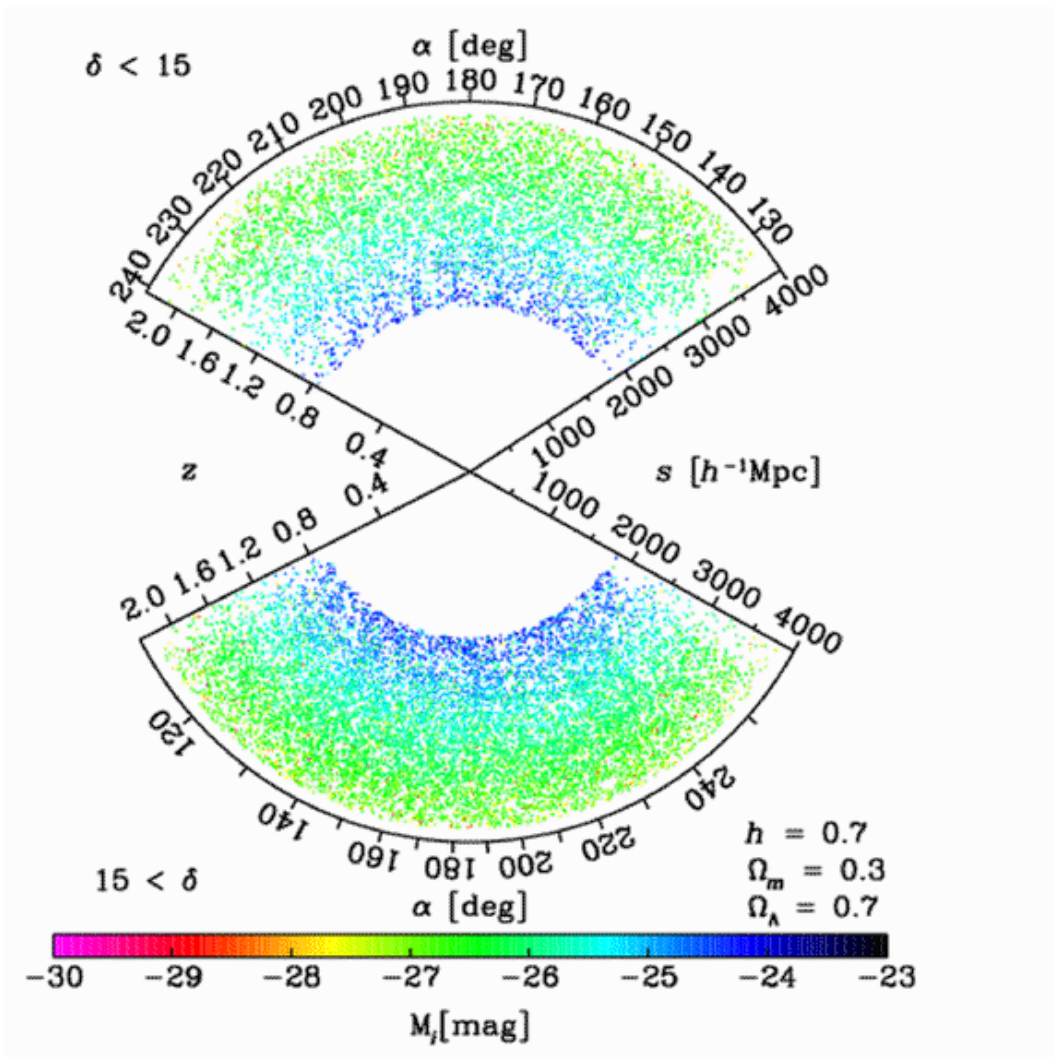
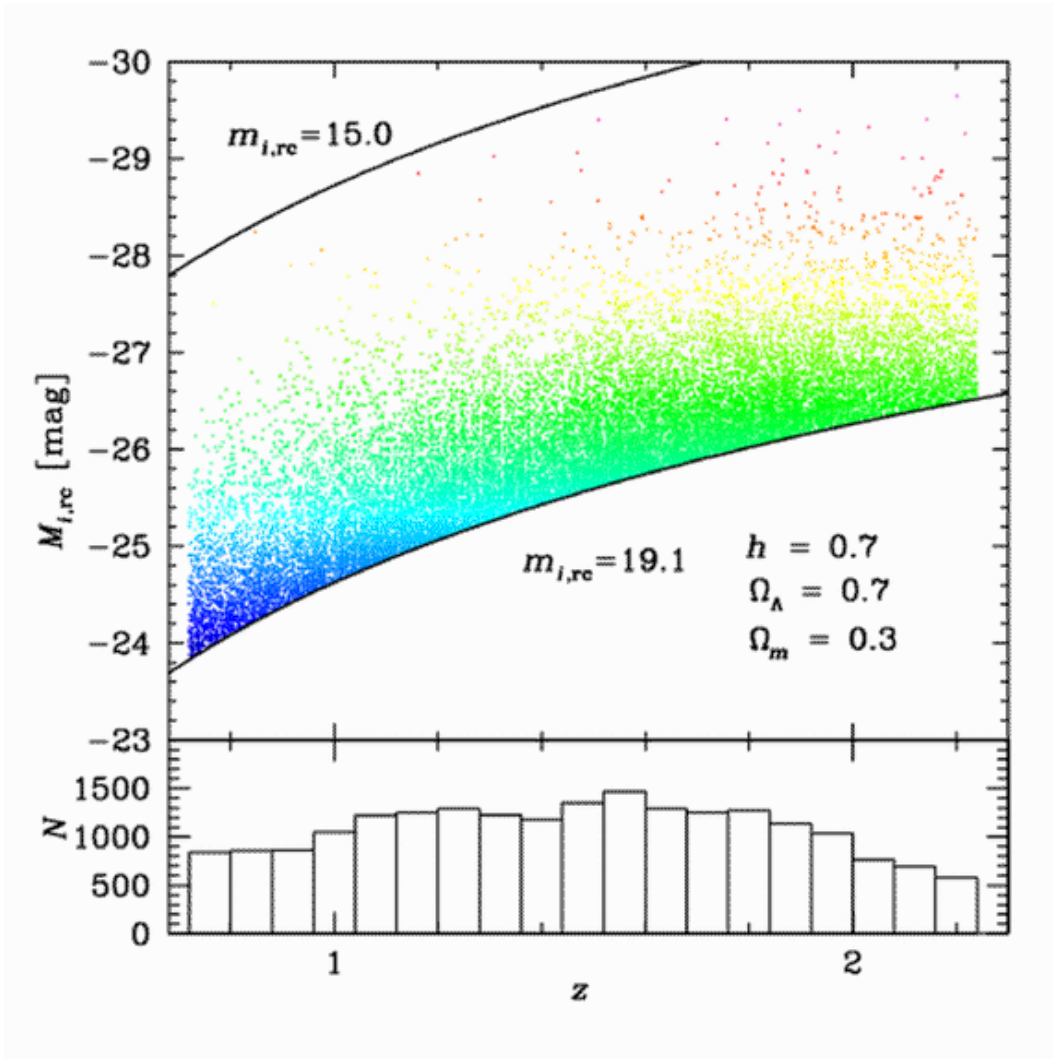
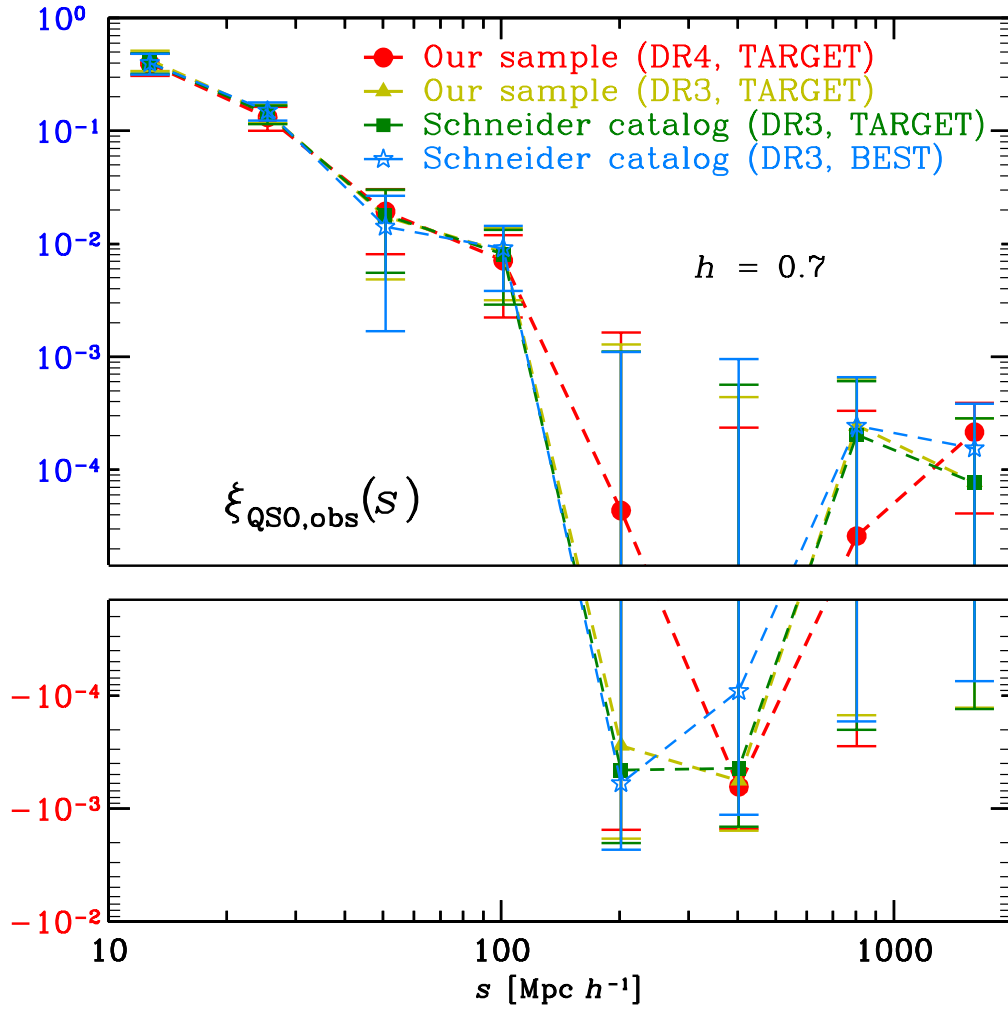


Fig. 2. Wedge diagram of the quasar distribution (19986 quasars in total for  $0.72 < z < 2.24$ ) corresponding to Figure 1.



**Fig. 3.** Scatter plot of redshift and  $i$ -band absolute magnitude (*Upper panel*) and the corresponding redshift histogram (*Lower panel*) of our quasar sample ( $0.16 \leq z \leq 2.24$  and  $15.0 \leq m_{i,rc} \leq 19.1$ ). The width of the redshift bin is 0.08. To compute the absolute magnitude, we assume that the energy spectrum of quasars follows a single power-law with a spectral index of  $-0.5$ , and adopt the cosmology of  $\Omega_m = 0.3$  and  $\Omega_\Lambda = 0.7$ .



**Fig. 4.** The two-point correlation functions of our samples, BEST DR3 and TARGET DR3 (the  $n = 1$  binning offset) for  $\Omega_m = 0.3$ ,  $\Omega_\Lambda = 0.7$  and  $h = 0.7$ . Filled circles and triangles correspond to our samples (DR4 and DR3), and filled squares and stars correspond to the BEST and TARGET DR3 quasar samples in the catalog by Schneider et al. (2005).

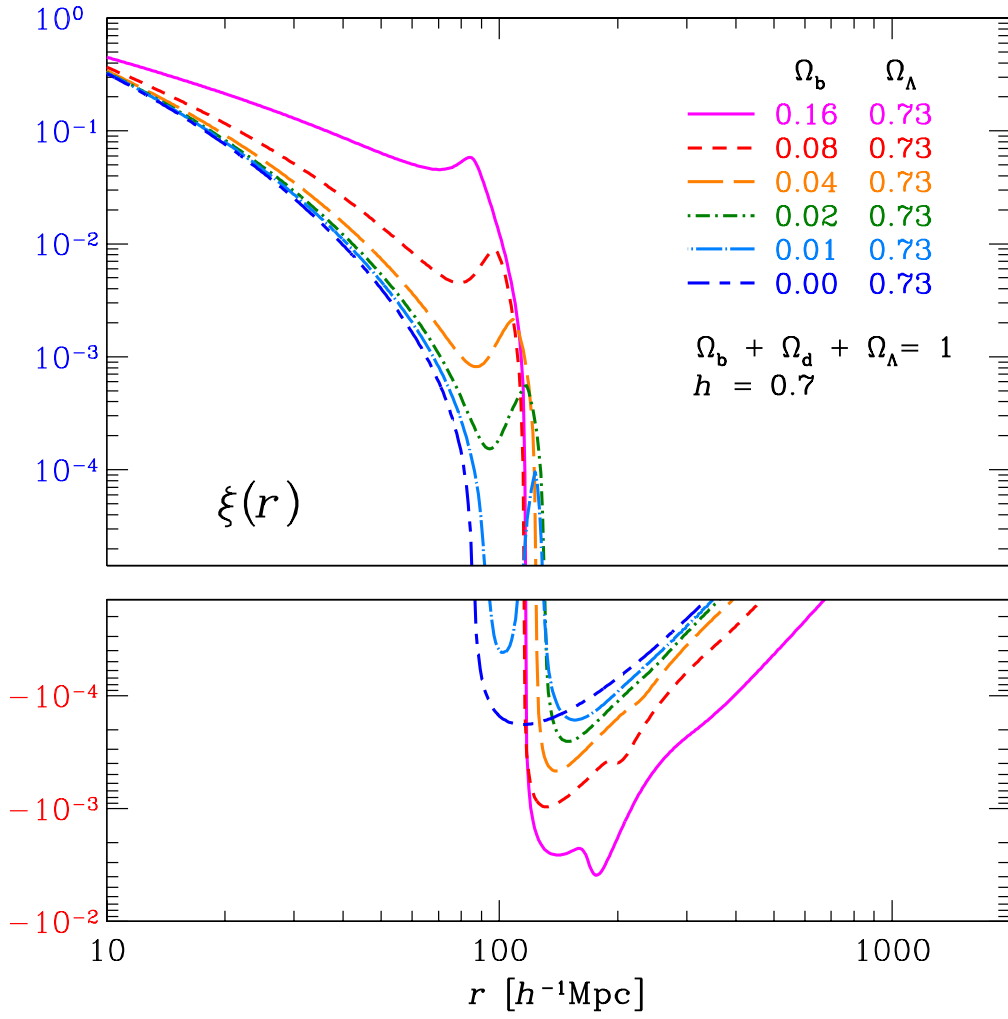


**Fig. 5.** Matter two-point correlation functions in linear theory (in real space) at  $z = 0$  for different values of  $\Omega_b$ . The CDM transfer function of Eisenstein, Hu (1998) is adopted. We assume the spatially flat model ( $\Omega_b + \Omega_d + \Omega_\Lambda = 1$ ), and  $h = 0.7$ .

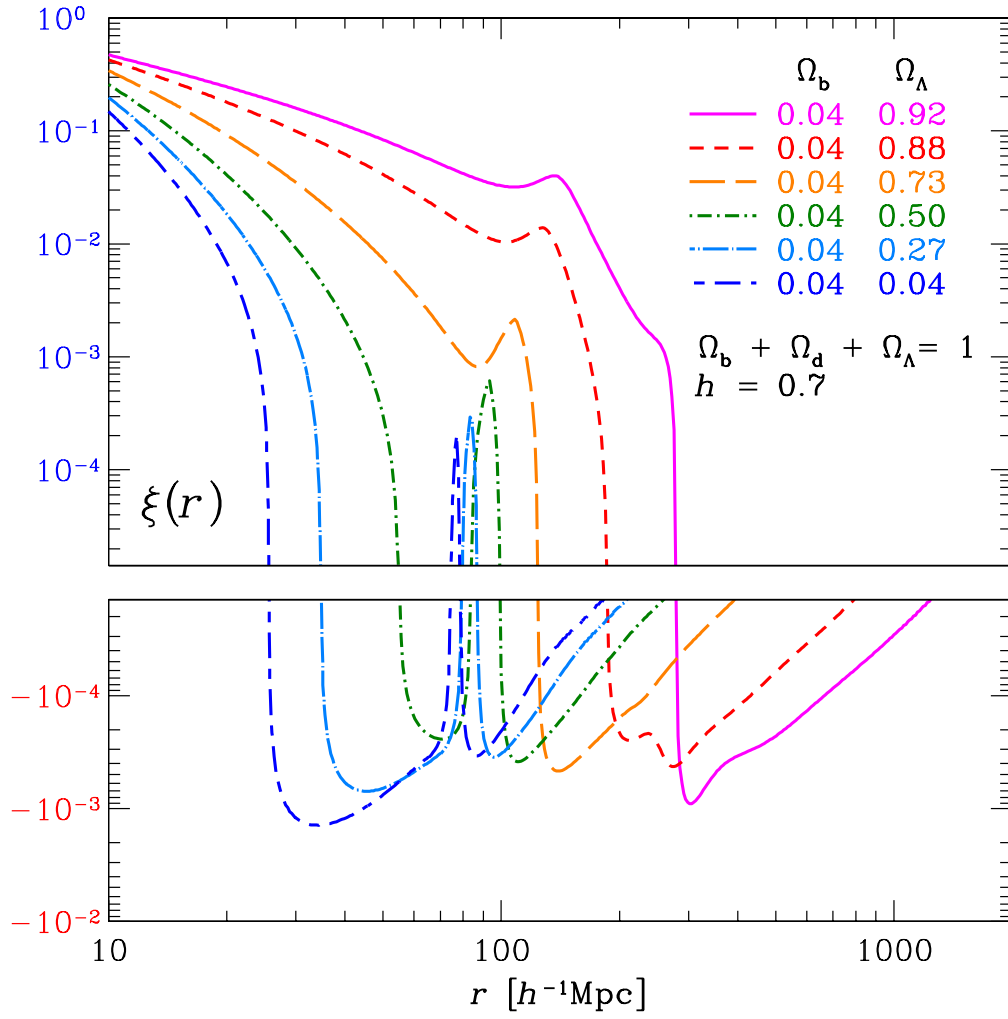
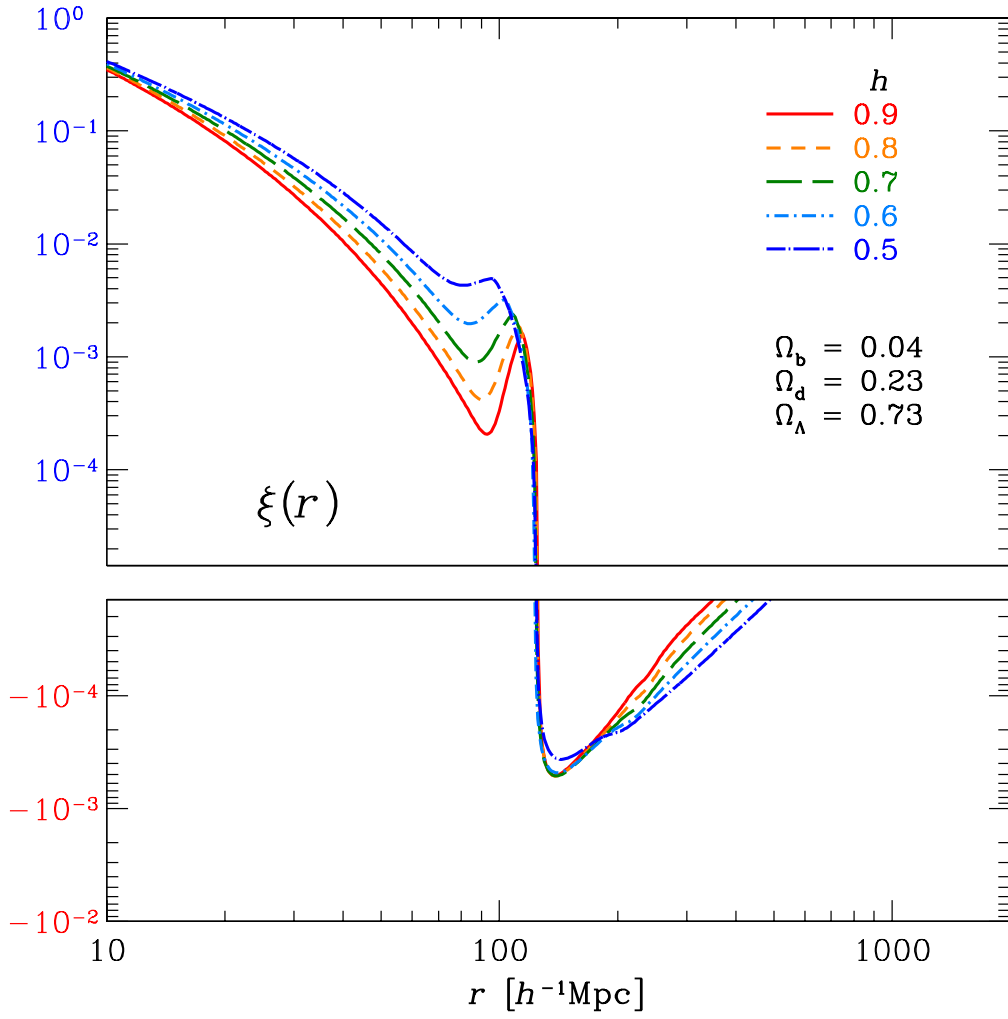


Fig. 6. Same as Figure 5 but for different values of  $\Omega_\Lambda$  with  $\Omega_b = 0.04$  and  $h = 0.7$ .



**Fig. 7.** Same as Figures 5 and 6 but for different values of  $h$  with  $\Omega_b = 0.04$ ,  $\Omega_d = 0.23$ , and  $\Omega_\Lambda = 0.73$ .

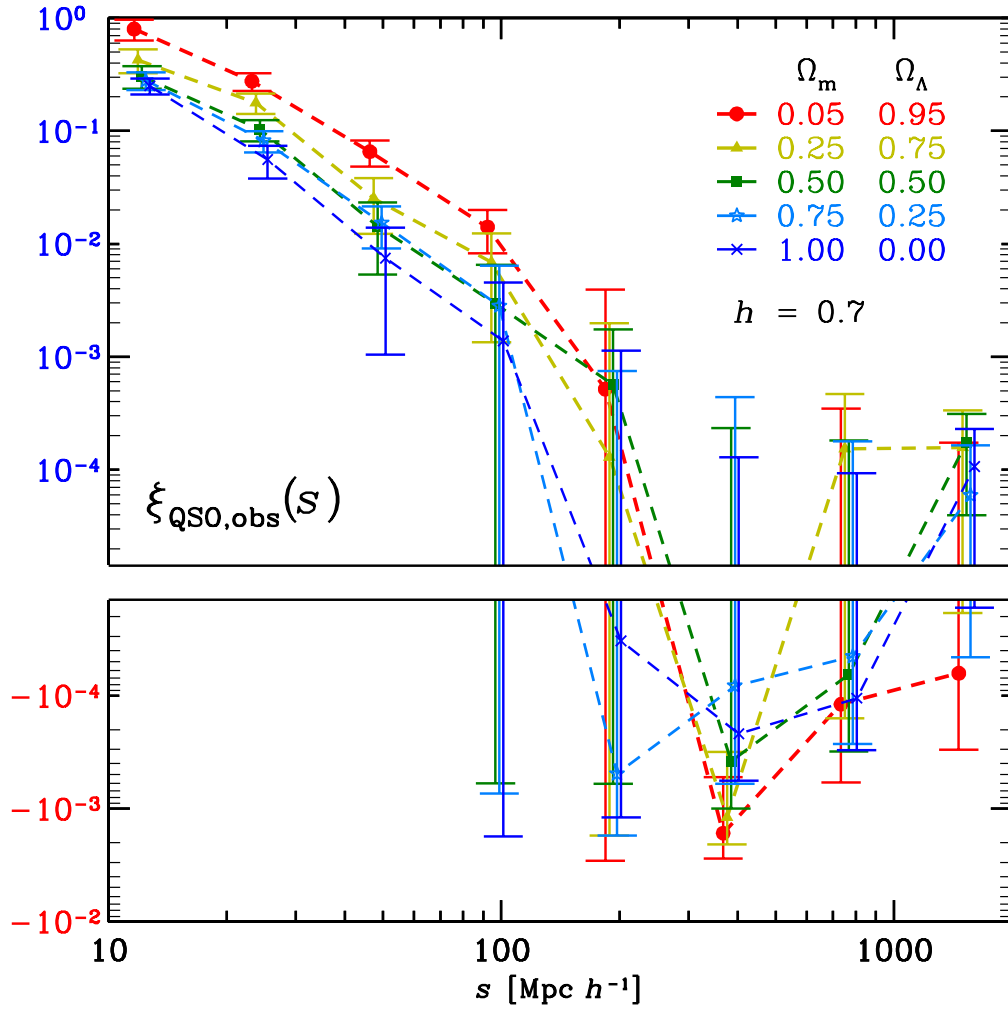
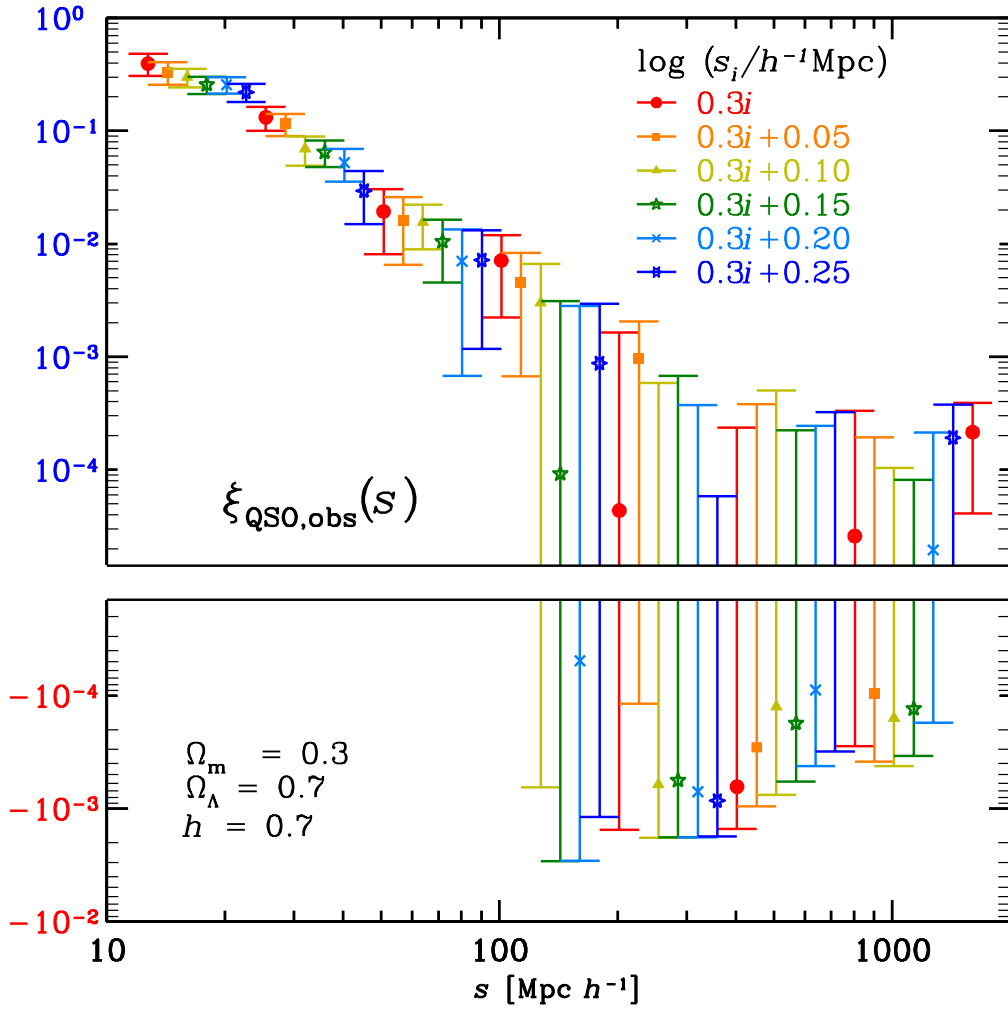
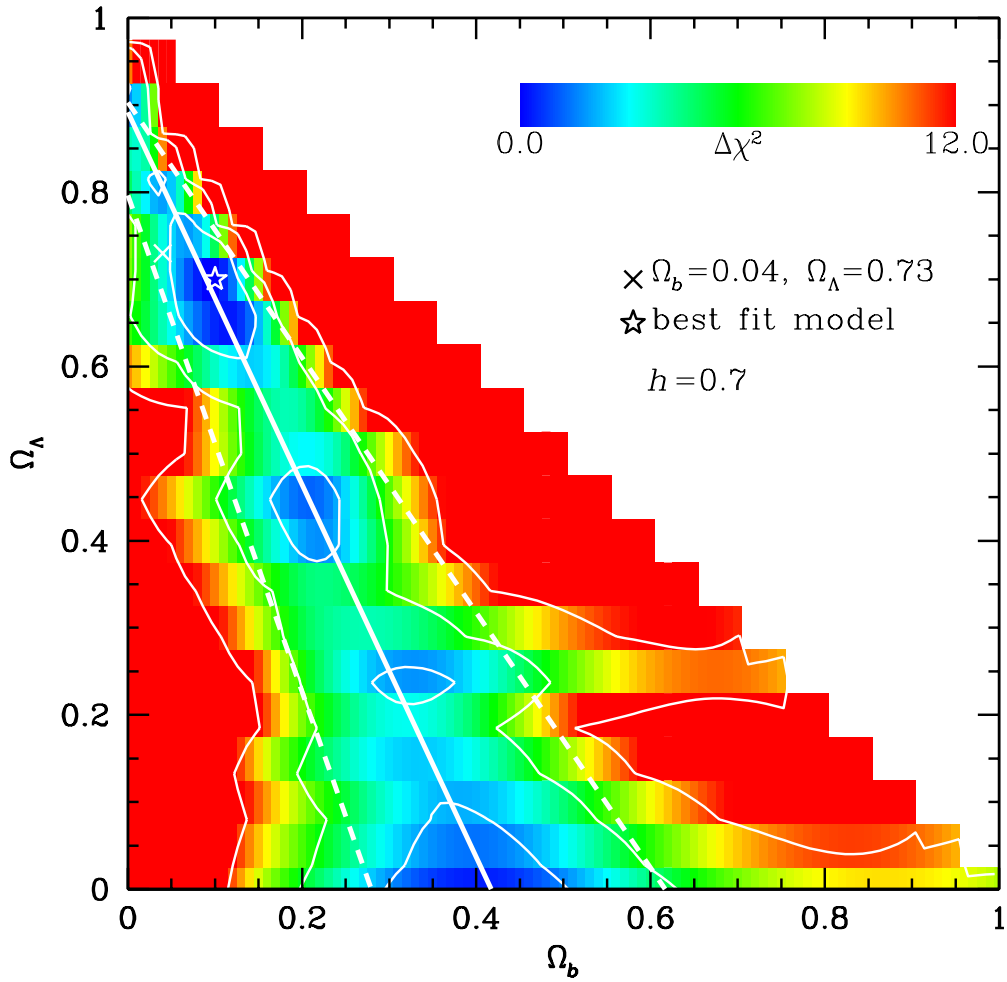


Fig. 8. The two-point correlation functions of SDSS quasars (the  $n = 1$  binning offset) for several different values of  $\Omega_\Lambda$  ( $h = 0.7$ ).



**Fig. 9.** The binning offset dependence of the two-point correlation functions of quasars. Results for the six different binning offsets (see eq.[2]) are plotted. We adopt  $\Omega_m = 0.3$ ,  $\Omega_\Lambda = 0.7$ , and  $h = 0.7$ .





**Fig. 10.** Contour plot of  $\Delta\chi^2$  (eq.[12]) on the  $\Omega_b - \Omega_\Lambda$  plane ( $h = 0.7$ ). The three contour curves represent the 68%, 95% and 99.7% confidence levels. The cross and the star indicate the values preferred by WMAP ( $\Omega_b = 0.04$  and  $\Omega_\Lambda = 0.73$ ), and our best-fit model ( $\Omega_b = 0.1$  and  $\Omega_\Lambda = 0.7$ ). We adopt the  $n = 1$  binning offset in equation (2). The solid and dotted straight lines indicate the linear fits to the mean and the  $2\sigma$  contour levels (eqs.[13] and [14]), respectively.

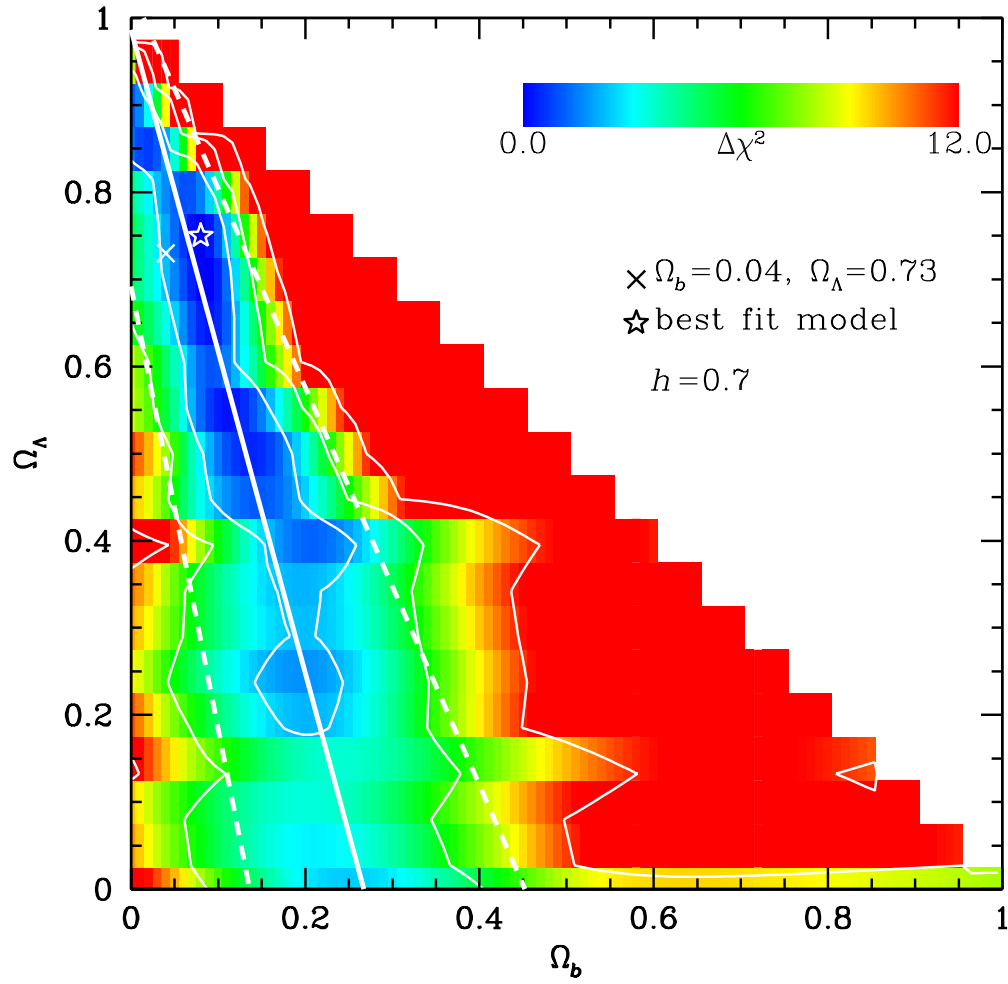


**Fig. 11.** Same as Figure 10 but for the  $n = 4$  binning offset. The solid and dotted straight lines indicate the linear fits to the mean and the  $2\sigma$  contour levels (eqs.[15] and [16]), respectively.

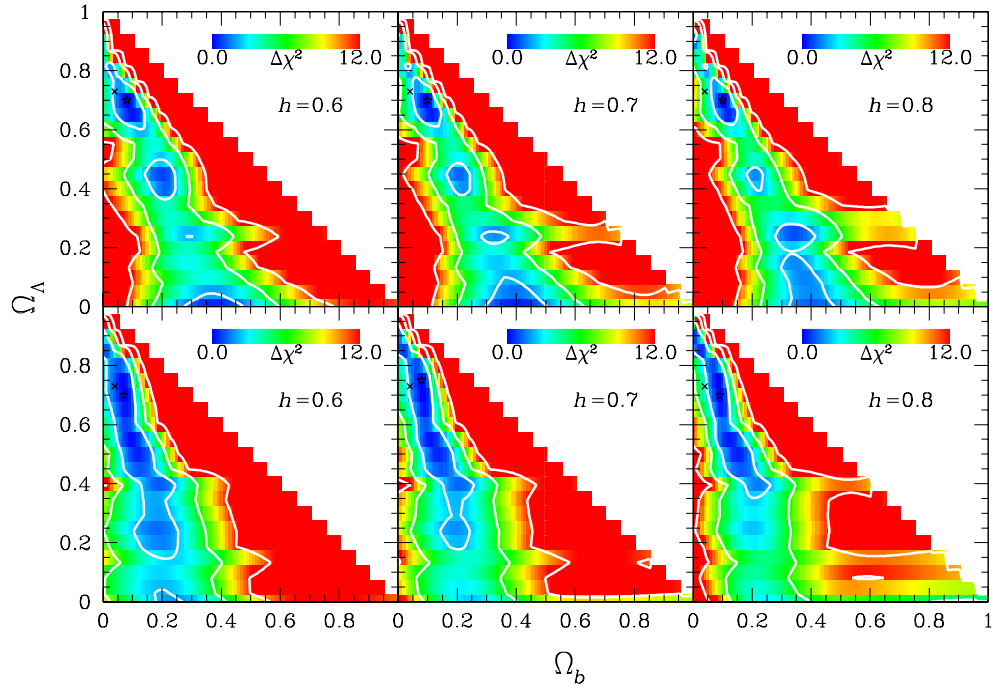


**Fig. 12.** Same as Figures 10 and 11 but for  $h = 0.6$  (Left panels),  $h = 0.7$  (Center panels), and  $h = 0.8$  (Right panels). Upper panels:  $n = 1$  and Lower panels:  $n = 4$  binning offsets.